Aerospace Science and Technology 158 (2025) 109895

Contents lists available at ScienceDirect

Aerospace Science and Technology

journal homepage: www.elsevier.com/locate/aescte

Main flight data on transpiration cooled sharp edge fins in hypersonic conditions on the sounding rocket HIFLIER

Giuseppe D. Di Martino [a,*], Jonas Peichl [a], Fabian Hufgard [b], Christian Duernhofer [b], Stefan Loehle [b], Johannes Göser [c]

[a] DLR Institute of Structures and Design, Pfaffenwaldring 38-40, 70569 Stuttgart, Germany
[b] High Enthalpy Flow Diagnostics Group, Institute of Space Systems, University of Stuttgart, Pfaffenwaldring 29, 70569 Stuttgart, Germany
[c] DLR Mobile Rocket Base (MORABA), Münchener Straße 20, 82234 Weßling, Germany

ARTICLE INFO

Communicated by Cummings Russell

Keywords:
Transpiration cooling
Ceramic matrix composites
Thermal protection system
Hypersonic flight experiment

ABSTRACT

Transpiration cooling is a promising thermal management technique that could be applied in hypersonic regimes to protect critical external structural components subjected to the highest aerothermal pressure and heat loads. In the framework of the HIFLIER program, a module of the sounding rocket scientific payload has been designed and setup to test the application of the transpiration cooling in real hypersonic flight conditions to sharp edge fins, whose leading edge is made of an innovative porous C/C-SiC material, so-called OCTRA. The module was integrated into a single-stage sounding rocket that was successfully launched into a parabolic trajectory reaching hypersonic conditions during ascent and during descent, with a maximum Mach number of 6.15. This paper presents the setup of the experimental system and its integration in the rocket module as well as the main collected flight data. The results validate the transpiration cooling technology, showing a good response of the system with a cooling efficiency of up to 40 % in hypersonic regime in both the ascent and the descent phases.

1. Introduction

Atmospheric entry vehicles or spaceplanes flying at hypersonic speed experience severe aerothermal loads [1]. Therefore, one of the most challenging aspects in the development of these vehicles is the design of suitable thermal protection systems (TPS) for the most critical components, especially in the cases in which the stability of the aerodynamic shape is needed, or for example when full reusability is required. In those cases, the use of ablative materials is to be excluded and sophisticated structures based on ceramic matrix composite materials, which can sustain very high temperatures and consequently can radiate back most of the convective heat, are currently the state of the art [2].

However, the application of these so-called passive TPS is limited by the materials' operational limit temperature, which, although very high, could be not sufficient, for example when the flight trajectory foresees a prolonged time in hypersonic regimes and, especially, on components with sharp edges, such as wing leading edges, stabilizer fins, and air intakes, where the strong, attached shock wave determines highly concentrated thermal loads [3]. In these cases, the capabilities of the hot structures must be extended and one option is the implementation of active cooling techniques.

Among the different active cooling techniques, a very promising solution is represented by transpiration cooling. Here, a coolant fluid is forced through a porous wall into the hot gas region. This leads to the double effect of convectively cooling the wall itself and lowering the convective heat transfer from the hot gas into the surface by mixing into the boundary layer, creating a protective cooling film [4]. First studies for the application of transpiration cooling up to supersonic Mach numbers date back to the 1950′s [5,6], showing a high potential for application in combustion chambers and gas turbines [7]. The application of transpiration cooling in combination with high temperature resistant permeable refractory ceramic matrix composite (CMC) materials, like carbon fiber reinforced carbon (C/C) allowed the extension of the capabilities of the technique also for application to rocket engine combustion chambers and hypersonic vehicles TPSs [8–10].

A further improvement of the abovementioned technology lies in the improvement of the oxidation resistance of the material. Here, the DLR Institute of Structure and Design (DLR-BT) has worked in the past ten years towards the development of a variant of the in-house developed C/C-SiC material with defined porosity level designed specifically for

* Corresponding author.
E-mail address: giuseppe.dimartino@dlr.de (G.D. Di Martino).

https://doi.org/10.1016/j.ast.2024.109895
Received 19 June 2024; Received in revised form 18 December 2024; Accepted 19 December 2024
Available online 20 December 2024

Fig. 1. HIFLIER sounding rocket launch (photo credit DLR MORABA).

transpiration cooling applications, denominated OCTRA (Optimized Ceramic for Hypersonic Application with Transpiration Cooling) [11]. So far, OCTRA has shown good potentialities for application on sharp leading-edge design [12], as well as in the context of investigating rocket engine combustion chamber cooling [13].

Ground test studies of the application of transpiration cooling in hypersonic flow regimes have been extensively performed in the last years [14–16]. Nevertheless, while on one side ground testing in controlled laboratory environments has a fundamental importance for improving the understanding of the technology and of the corresponding phenomena involved, on the other side it presents inevitably specific limitations which do not allow to completely duplicate the flight environment [17,18]. Therefore, performing successful flight experiments and collecting reliable data ultimately represents an essential step to complement the know-how of the technologies and their full qualification. In particular, sounding rocket hypersonic flight experiments play a key role on one side for improving the readiness level of the tested technologies and on the other side to generate an extensive reliable database, which can be made available to the scientific community for tuning and validating high-fidelity numerical models and reliable design tools [19–21]. The only flight experiment on transpiration cooling on a hypersonic sounding rocket was performed in the SHEFEX II mission [22]. Here, the technique was applied to a flat probe of porous C/C material integrated into the TPS of the rocket forebody, showing, although for a short time before losing signal, a very promising response.

In the present paper, a new transpiration cooling flight experiment is presented, with the objectives of collecting flight data of transpiration cooling to fins with sharp leading edge and for investigating the usability of the newly developed OCTRA material in the hypersonic flight regime. For these purposes, a sounding rocket module, in the following denominated FinEx (Fin Experiment) module, has been developed, hosting four CMC fins with a porous OCTRA leading edge connected to a nitrogen gas supply system, and integrated on the sounding rocket HIFLIER (Hypersonic International Flight Research Experimentation). The HIFLIER rocket was successfully launched in collaboration with the Swedish Space Corporation (SSC) from Esrange Space Center in Kiruna (Sweden) on the 10th October 2023. After a brief description of the HIFLIER mission and flight trajectory, an overview of the FinEx module design is given, including the full characterization of the fin's permeability. The main flight measurements are then presented in the following.

2. HIFLIER configuration and flight trajectory

As mentioned above, the FinEx module was integrated on the HIFLIER launch vehicle, a single-stage, unguided, rail-launched sounding rocket propelled by the solid propellant Black Brant V rocket motor from the Canadian company Magellan Aerospace. A picture of the HIFLIER rocket during launch is shown in Fig. 1.

In particular, the FinEx module was positioned after the experimental forebody, a smooth (no intentional roughness) cone with a semi-aperture angle of 7° dedicated to the investigation of boundary layer transition onset, the transition module (TSM), a truncated cone segment connecting the final section of the conical forebody to the 14 inch diameter section of the rest of the payload, and the payload support module (PSM), a circular interface adapter where also an onboard camera was located. The schematic of the scientific payload is shown in Fig. 2.

The flight trajectory data of the HIFLIER sounding rocket were measured by a DMARS-R (Digital Miniature Attitude Reference System) inertial measurement unit (IMU) [23]. Fig. 3 shows the measured flight altitude, with an apogee of around 190 km, flight velocity and Mach number.

For altitudes below 75 km the ambient pressure p_a and temperature T_a is directly obtained from the altitude H assuming the U.S. standard atmosphere model (COESA76) [24]. This model is used, because the experiment was mostly performed for altitudes below 75 km and is still in the continuous flow regime (see Fig. 3b and 3c). Assuming ideal gas behavior, the flight Mach number can be determined using the measured velocity V_∞. Around $T + 414$ s there was the motor separation marking the end of the flight experiment.

In order to reduce the amount of coolant gas needed, the

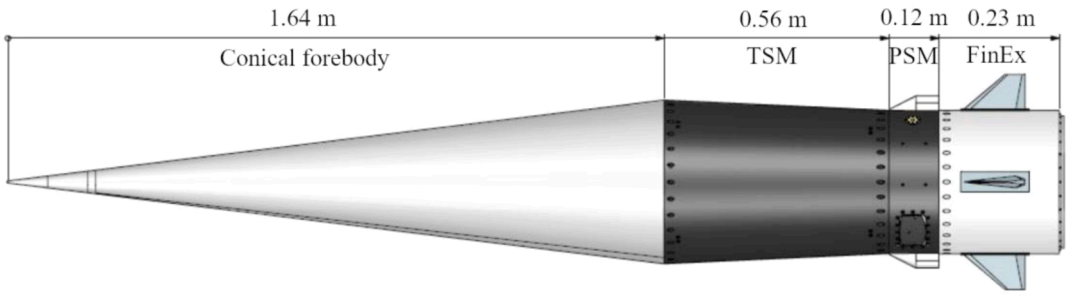

Fig. 2. Scientific payload of the HIFLIER sounding rocket.

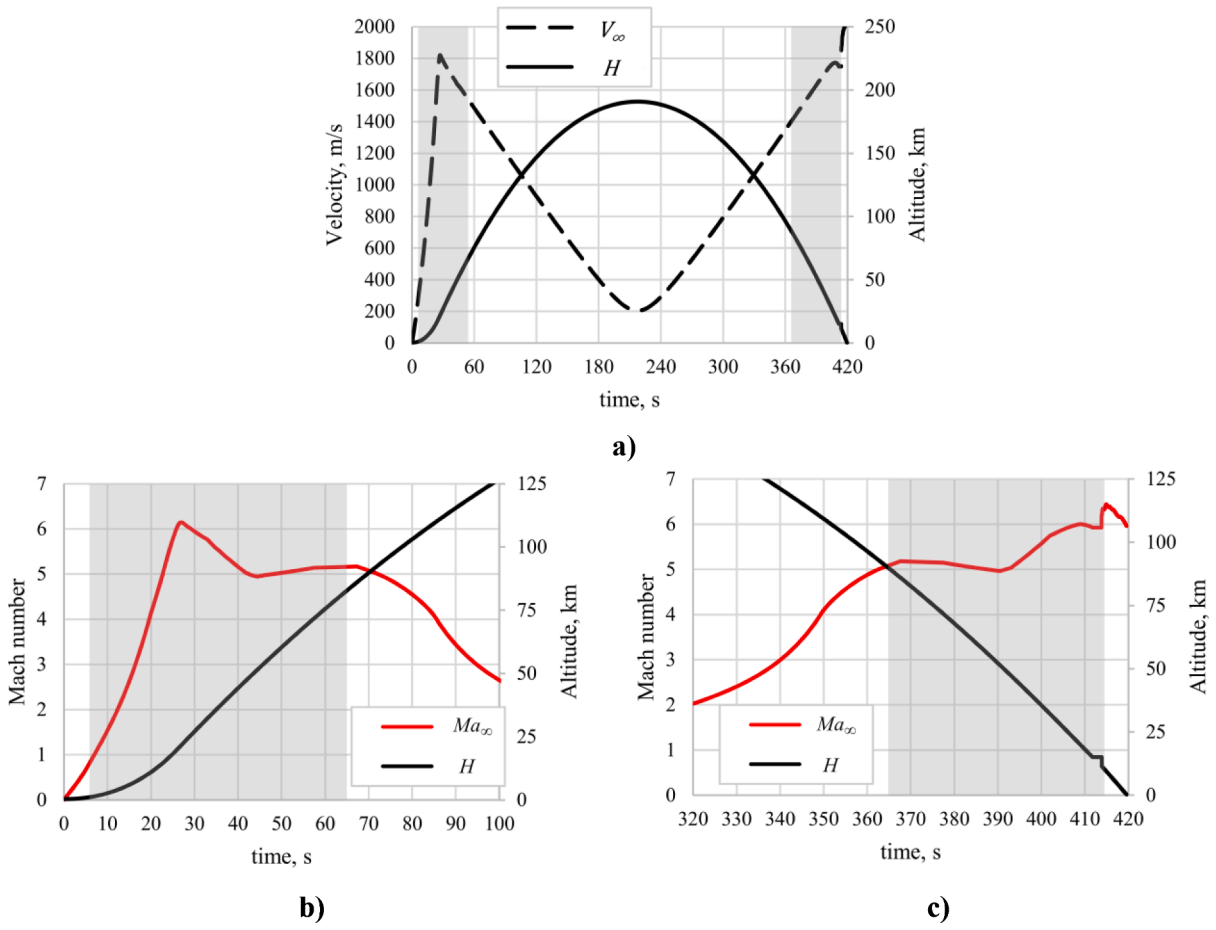

Fig. 3. HIFLIER sounding rocket flight trajectory; the experimental time windows for the activation of the FinEx transpiration cooling are marked in grey.

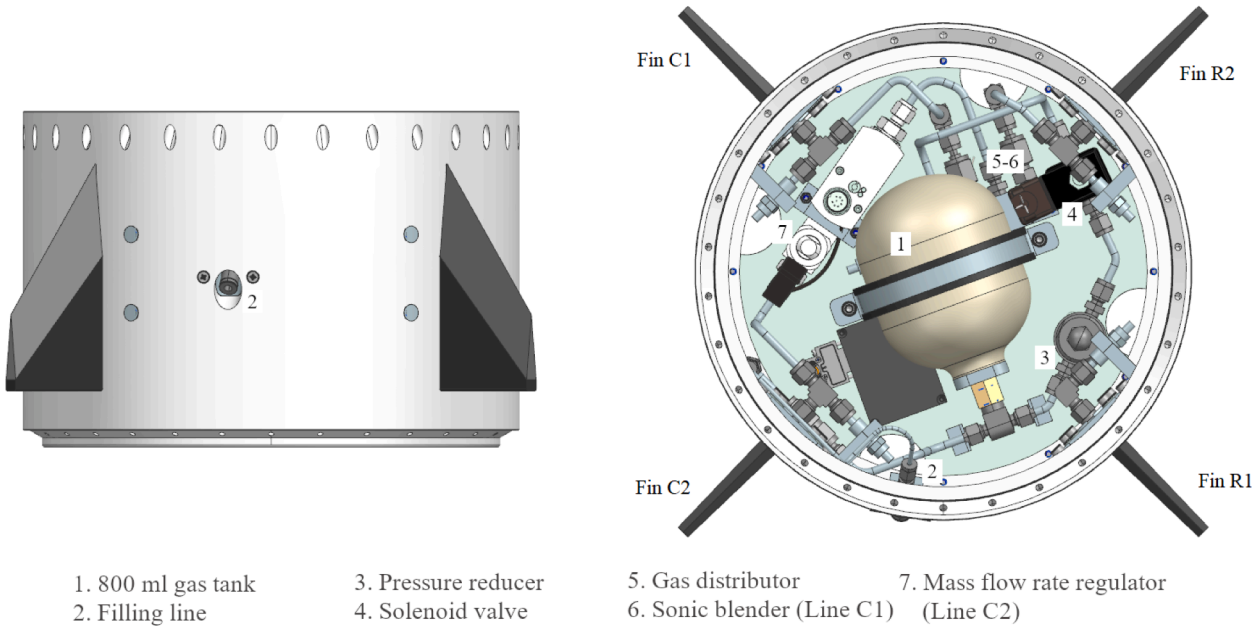

Fig. 4. FinEx II module overall design.

transpiration cooling on the FinEx module was activated in two different experimental windows, during ascent between $T + 5$ s and $T + 55$ s and during descent from $T + 365$ s until $T + 415$ s (highlighted in grey in Fig. 3 and in the next graphs), corresponding to the time of atmospheric flight in the hypersonic regime, when the fins are subjected to the highest aerothermal loads [25].

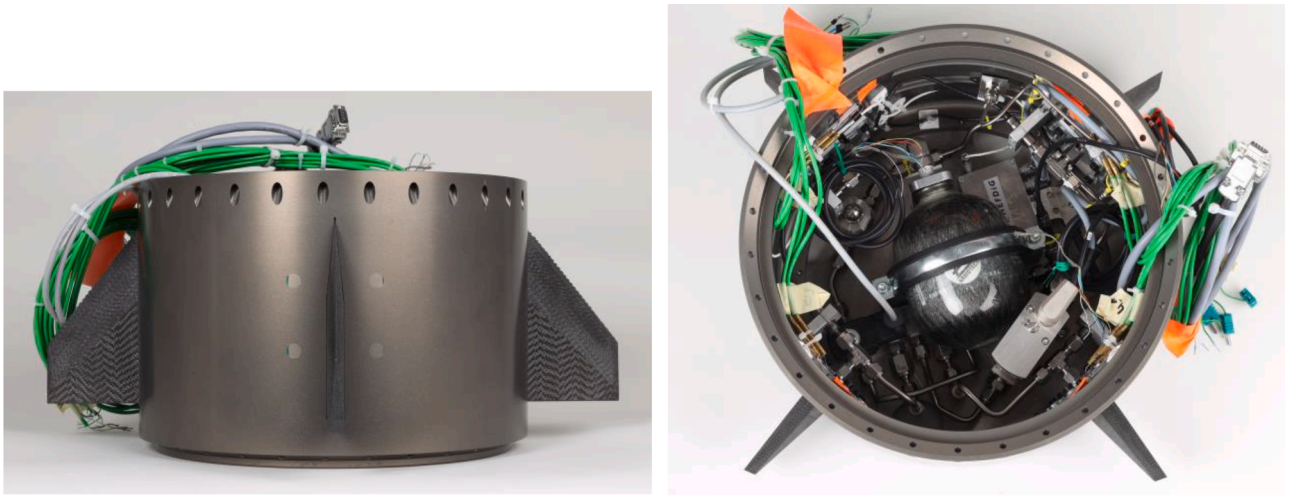

a) Side view b) Top view

Fig. 5. FinEx II module fully assembled.

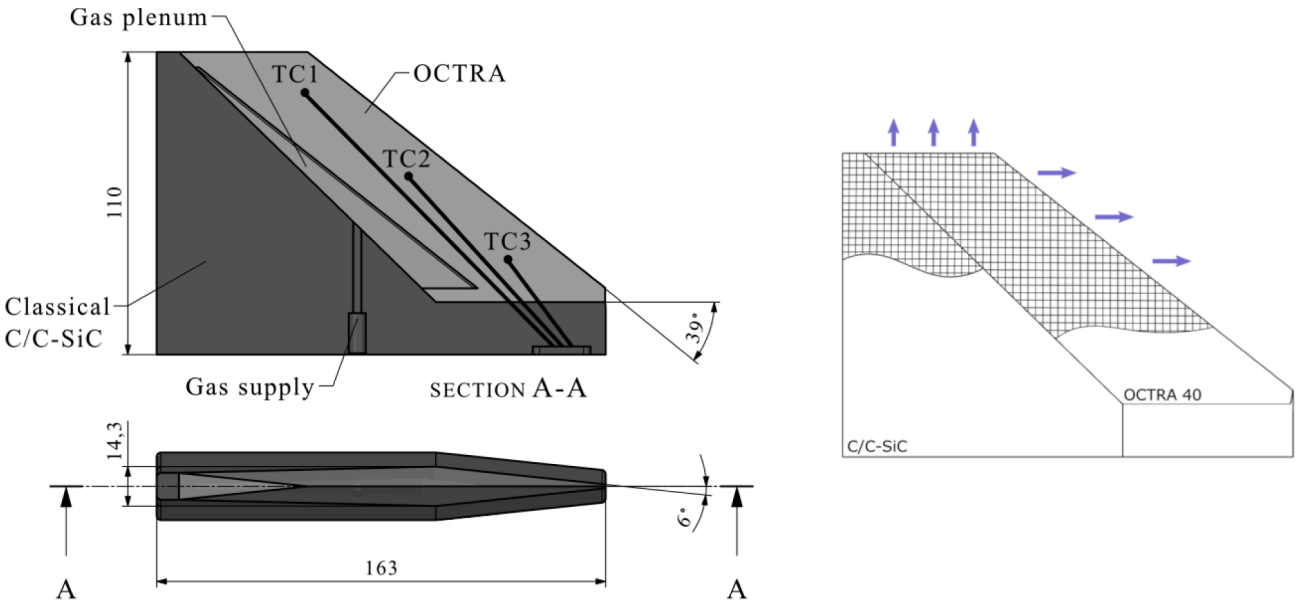

a) Fin design b) Fibers orientation

Fig. 6. Design of the CMC fin with porous leading edge.

3. FinEx module design overview

Fig. 4 shows the design of the FinEx module, which is equipped with four identical fins, each pair of diametrically opposite fins exposed to the same flow conditions. Fig. 5 shows pictures of the FinEx module fully assembled, before its integration on the HIFLIER rocket.

A detailed description of the fins design, the gas system configuration and the operating conditions is given in the following. For more details refer also to [25,26].

3.1. CMC fins with porous leading edge for transpiration cooling

As mentioned before, in the present flight experiment CMC fins are employed foreseeing the application of the so-called OCTRA material, which is a porous version of the typically used C/C-SiC material. While classical C/C-SiC material produced via liquid silicon infiltration is almost impermeable, OCTRA is obtained by including a predefined amount of aramid fibers in the carbon-fiber reinforced plastic (CFRP) preform. The aramid fibers thermally degrade during pyrolysis generating larger pores that are not completely filled during the silicon infiltration. In this way, the permeability level can be defined based on the amount of aramid fibers included in the CFRP preform. More info on the OCTRA material, the manufacturing process and the characterization of the main material properties can be found in [11].

Fig. 6 shows the overall design of the CMC fin. In order to concentrate the cooling in the region of the leading edge, where the higher aerothermal loads and consequently temperatures are expected, only the forward part of the fin is made of the permeable OCTRA material (displayed in light grey in Fig. 6a), while the remaining part is made of classical impermeable C/C-SiC (in dark grey in Fig. 6a). The two parts are joined together according to the process described in [27].

Taking into account that in the manufacturing process of the OCTRA

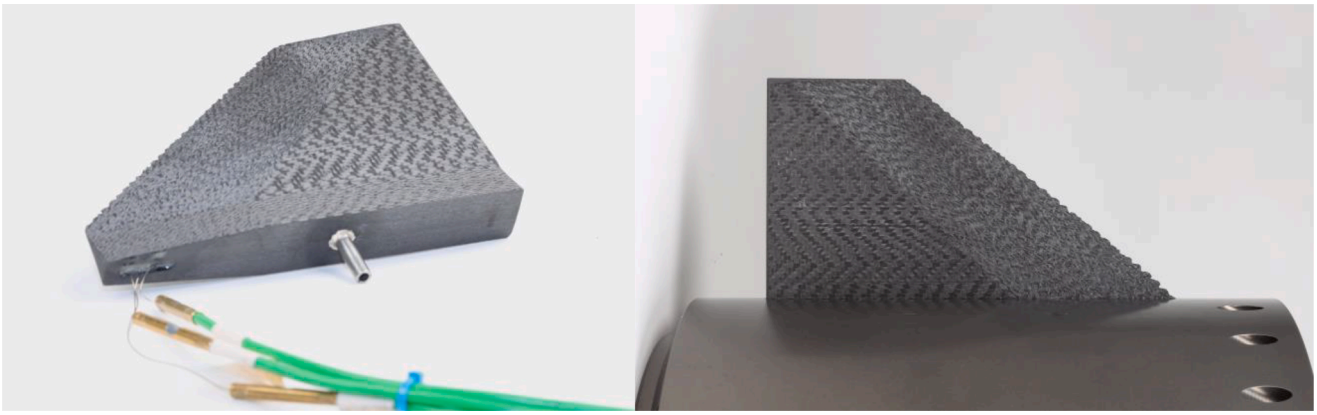

Fig. 7. Pictures of the CMC fin: a) fin with soldered tube for coolant feeding and glued thermocouples; b) fin integrated in the FinEx module.

material the main orientation of the pores is determined by the aramid fibers in the CFRP precursor, the latter was produced using two-dimensional mixed carbon/aramid fiber plies resulting in a main orientation of the pores parallel to the chosen fiber orientation, as shown in Fig. 6b. Moreover, in the present work the OCTRA40 variant of the material was adopted, indicating a 40 % vol percentage of aramid fibers in the CFRP preform leading to a porosity of around 8–9 % in the final siliconized state.

With reference to Fig. 6a, inside the permeable leading edge, a plenum volume for the cooling gas is foreseen. The coolant, which in this case is gaseous nitrogen, is fed through the gas system described in Section 3.3 into the plenum through a hole in the C/C-SiC component in which a 6 mm stainless steel tube is soldered. This assures also the sealing at the operating pressure building inside the plenum as an effect of the permeability characteristics of the porous material, as it will be described in Section 3.2 and in Fig. 13.

Three type-K thermocouples for measuring the in-depth material temperature were glued with graphite-based paste (Graphi-Bond 669) inside the leading edge of each fin to monitor the thermal response, at the nominal position indicated in Fig. 6a.

Pictures of the CMC fin are shown in Fig. 7.

3.2. Characterization of the fins' overall permeability

The permeability of the fins' leading edge plays a fundamental role in the transpiration cooling application. It is characterized in terms of the Darcy-Forchheimer equation, which in the formulation by Innocentini et al. [28] describes the pressure loss of a fluid through a porous medium as:

$$\frac{p_{cg,in}^2 - p_{cg,out}^2}{2p_{cg,out}L_{ch}} = \left(\frac{\mu_{cg}}{K_D}\right)u_D + \left(\frac{\rho_{cg}}{K_F}\right)u_D^2 \tag{1}$$

where $p_{cg,in}$ and $p_{cg,out}$ are the coolant gas pressure at the inlet and outlet of the porous medium respectively, μ_{cg} and ρ_{cg} are its viscosity and density, L_{ch} is the characteristic length of the porous medium and K_D and K_F are the Darcy and Forchheimer coefficients. The superficial Darcy velocity u_D can be derived from the coolant mass flow rate via the continuity equation:

$$u_D = \frac{\dot{m}_{cg}}{\rho_{cg}A_c} \tag{2}$$

where $\dot{m}_{cg}$ is the coolant mass flow rate and A_c is the outflow area.

In the present work, the permeability measurements were carried out at the AORTA (Advanced Outflow Research Facility for Transpiration Application) facility at DLR-BT [13]. The facility comprises of three parallel gas lines, which can be opened and closed by pneumatically driven valves. Each line includes a Bronkhorst CORI-FLOW mass flow controller M12, M14 and M55 respectively, each optimized for a certain range of mass flow rates. P33X-series pressure gauges (uncertainty of 0.05 % FS) and type-K thermocouples are used to measure the inlet and outflow pressures and temperatures at steady state conditions for different values of the cooling gas mass flow rate. K_D and K_F are then obtained by fitting the measured data according to Eq. (1), using a least squares algorithm.

Table 1
Darcy and Forchheimer coefficients of the transpiration cooled fins.

	Fin C1	Fin C2	OCTRA cyl. sample [26]
Darcy coefficient K_D, m^2	$1.76{\cdot}10^{-12} \pm 1.5{\cdot}10^{-13}$	$1.57{\cdot}10^{-12} \pm 1.2{\cdot}10^{-13}$	$1.62{\cdot}10^{-12}$
Forchheimer coefficient K_F, m	$2.30{\cdot}10^{-8} \pm 1.2{\cdot}10^{-9}$	$2.44{\cdot}10^{-8} \pm 1.4{\cdot}10^{-9}$	$4.5{\cdot}10^{-7}$

The characterization of the permeability was first performed on a cylindrical sample taken from the same OCTRA material batch from which the fins' leading edges have been manufactured, as described in [26]. In second place, separate measurements have been conducted for each fin. Steady-state pressure measurements were conducted by feeding the specified mass flow rate of gaseous nitrogen into the investigated fins in the range 0.1–1.5 g/s, and measuring the plenum and the ambient pressures and temperatures. The pressure gauges used have a range from 0.8 to 1.2 bar for ambient pressure and 0–300 bar for feeding gas pressure.

It is worth noticing that, compared to the cylindrical shape, the complex fin geometry results in a modified definition of the outflow area A_c and characteristic length L_{ch}. The values considered here are $L_{ch} =$ 38 mm for the characteristic length and $A_c = 2.69{\cdot}10^{-3}m^2$ for the area, given by the sum of the projections of the leading-edge area in the planes perpendicular to the fibers direction.

Table 1 summarizes the results in terms of K_D and K_F and the corresponding uncertainties for the fins C1 and C2, together with the reference values measured for the OCTRA material.

3.3. FinEx cooling gas feeding system and nominal operating conditions

Fig. 8 shows the schematic of the feeding line for the coolant gas employed on the FinEx module. Gaseous nitrogen was employed as the coolant gas. The corresponding components in the CAD model can be seen in Fig. 4b.

The gas is contained in an 800 ml volume gas tank (ARMOTECH, 1) at an initial pressure of around 250 bar The top-up of the tank is carried out during the flight countdown at T-2h30 min through the dedicated filling line (2), including an intake valve, a Swagelok® filter to avoid any contamination of the gas in the system and a check valve.

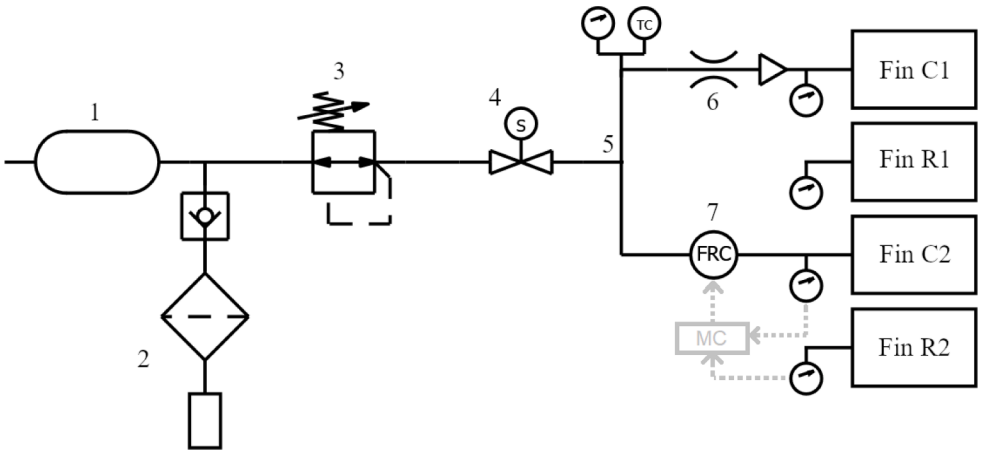

Fig. 8. FinEx cooling gas feeding line schematic.

Table 2
Transpiration cooling operating mass flow rates for the different fins.

Fin R1	Fin C1	Fin R2	Fin C2
No cooling Reference for fin C1	0.85 g/s	No cooling Reference for fin C2	CATS method

The nominal operating pressure for the transpiration cooling system is set with a pressure reducer (Swagelok®, 3), which is followed by the solenoid valve (Bürkert 6013, 4) to open the feeding line via an electric signal during the prescribed experiment windows. At this point, the actual gas pressure and temperature are measured by a Kulite® HKL-T-312 sensor.

After that, the gas is split into two different lines through a dedicated component (5). The first line leads the coolant gas to the fin C1 with a constant mass flow rate set by a blender operating in choked conditions (M = 1 at the throat) (6). The resulting system with the blender was preliminary calibrated in order to get a measurement of the actual mass flow rate based on the measurements of the total pressure and temperature.

The second line feeds the coolant gas to the fin C2, which on the other side is dedicated to the experiment in real flight conditions of the so-called Cooling Adjustment for Transpiration Systems (CATS) technique, in which the mass flow rate of the cooling gas is adjusted in real time according to the instantaneously measured actual surface heat flux during flight [29]. Therefore, in this case, a mass flow rate regulator (Bronkhorst® IN-FLOW F-201AI, 7) is included, which is in turn connected to the electronic box in which the CATS controller is implemented. More details about the CATS technique concept and the calibration for the present system can be found in [25,29]. The detailed results of the operation and the response of the CATS control during the HIFLIER flight are still under post-processing and will be the subject of a following paper. In the present work, just the directly measured data concerning the operating mass flow rate and the thermal response of the fin will be presented.

With reference to Fig. 4, the nominal transpiration cooling operating conditions for the different fins are summarized in Table 2.

Combined pressure and resistance temperature detector (RTD) sensors, Kulite® HKL-T-312 (uncertainty of 0.1 % FS) on fins R1 and C1, Kulite XTL-190SM-700kPaA (uncertainty of 0.1 % FS) on Fin R2 and Kulite HKL-T-1–235 M (uncertainty of 0.1 % FS) on fin C2, are included upstream of each fin to measure the corresponding gas pressure and temperature in the plenum.

4. Flow conditions estimation at the FinEx module

A simplified estimation of the flow conditions at the FinEx module around the abovementioned experimental time windows can be obtained by a 1D analytical flow field calculation for the known rocket geometry and the measured flight conditions.

Starting from the flight conditions described in Section 2, the fluid dynamic conditions on the conical forebody can be estimated by solving at each time for the given asymptotic conditions the corresponding

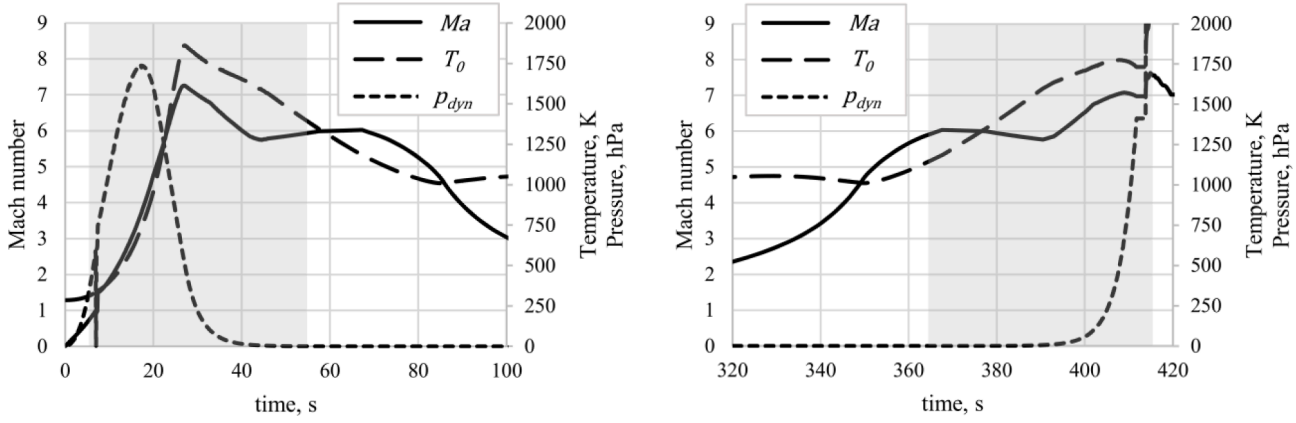

Fig. 9. Flow conditions at the FinEx module; the time windows for the activation of the FinEx transpiration cooling are highlighted in grey.

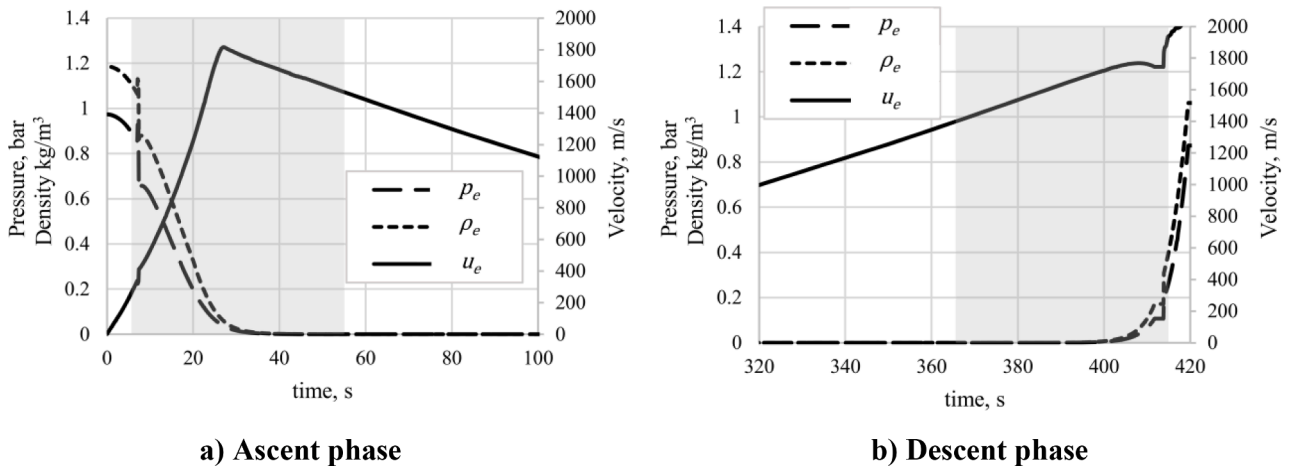

Fig. 10. Flow condition at the fin boundary layer edge.

conical shock wave forming in front of the tip. In this work, the approximate solution proposed in [30] is implemented.

Successively, the flow expands at the interface between the forebody cone and the TSM and the corresponding flow conditions are calculated with the classical Prandtl-Meyer expansion model. At this point, the shock wave at the PSM was estimated to have a negligible effect since it affects only a small region of the fins due to its low inclination (especially at the higher Mach number) and close position.

The resulting flow conditions at the FinEx module are shown in Fig. 9 in terms of Mach number Ma, total temperature T_0, and dynamic pressure p_{dyn}.

Finally, with a similar approach, the boundary layer edge conditions around the fins are estimated as the conditions downstream of the oblique shock wave forming in front of the fin's leading edge, where the upstream conditions are the ones estimated at the FinEx module as described above. The resulting flow conditions are shown in Fig. 10 in terms of velocity u_e, pressure p_e and density ρ_e.

It is worth noticing that the flow on the fins C1 and R1 (Fig. 4) was affected during some phases of the flight by the effect of the camera's external case (and the similar dummy case located on the opposite position for the sake of symmetry), which were located in front of the mentioned fins circumferentially rotated by an angle of 15°

5. Data acquisition and derived variables

As described in the previous section, the instrumentation present on the FinEx module allows for direct measurement of the feeding pressure and temperature of the coolant gas as set by the pressure reducer, the pressure and temperature inside the plenum of each fin and the in-depth material temperature in the fins' leading edge.

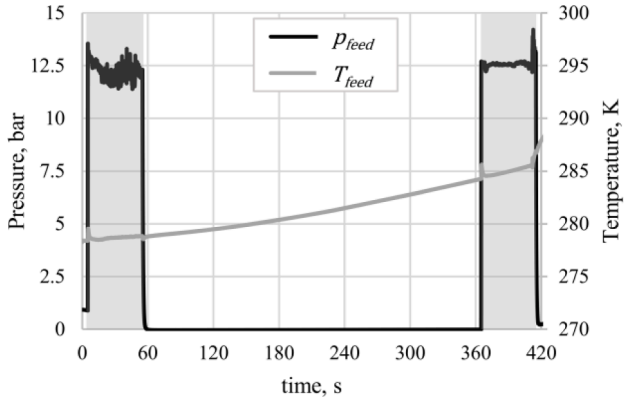

Fig. 11. Feeding pressure and temperature in the FinEx cooling gas system during the flight.

The signals of the pressure transducers and the thermocouples had a sample rates of 406.9 Hz and were sampled at 24bit resolution for inclusion into the telemetry.

For the fin C1 the mass flow rate of the coolant gas is obtained from the measurements of the feeding pressure $p_{0,cg}$ and temperature $T_{0,cg}$ as:

$$\dot{m}_{cg} = k\frac{p_{0,cg}}{\sqrt{T_{0,cg}}} \tag{3}$$

where the constant k is obtained from a calibration of the blender along the line and also includes the pressure loss effect with respect to the case of a de Laval shape. For the fin C2, the mass flow rate is also directly measured by the mass flow rate controller.

Assuming that the cooling flow through the porous material behaves as an ideal gas and considering the Sutherland law for the dynamic viscosity, Eqs. (1) and (2) for the fluid temperature exiting the porous wall $T_{cg,out}$ [31]. In particular, $\dot{m}_{cg}$ and $p_{cg,in}$ are the measured coolant mass flow rate and plenum pressure in the cooled fin, $p_{cg,out}$ is the external pressure at the fin's boundary layer edge, calculated as described in Section 2, and the values of the coefficient k_D and k_F are reported in Table 1. From this result and assuming that the temperature increases linearly in the porous wall, an estimation of the advective heat flux in the porous material, i.e. the heat absorbed by the cooling gas through convection inside the material pores, is given by:

$$\dot{q}_{adv} = \frac{\dot{m}_{cg}}{A_c} c_{p,cg}\left(T_{cg,out} - T_{cg,in}\right) \tag{4}$$

where $c_{p,cg}$ is the cooling gas specific heat and $T_{cg,in}$ is the cooling gas temperature measured inside the plenum.

The transpiration cooling is typically described in terms of two characteristic numbers, which are the blowing ratio F and the transpiration cooling efficiency Φ.

The blowing ratio F is defined as the ratio of the coolant mass flux on the transpiration outflow area and the hot gas boundary layer mass flux:

$$F = \frac{\rho_{cg}u_{cg}}{\rho_e u_e} = \frac{\dot{m}_{cg}/A_c}{\rho_e u_e} \tag{5}$$

where ρ_e and u_e are the density and the velocity of the flow at the boundary layer edge, calculated as described in Section 4, and A_c is the outflow area of the coolant, as defined in Section 3.2.

Given the strongly transient character of the present flight experiment and in order to relate the cooling efficiency to the directly measured data, a nondimensional temperature ratio is used in this work to describe the transpiration cooling efficiency Φ, similarly to what was

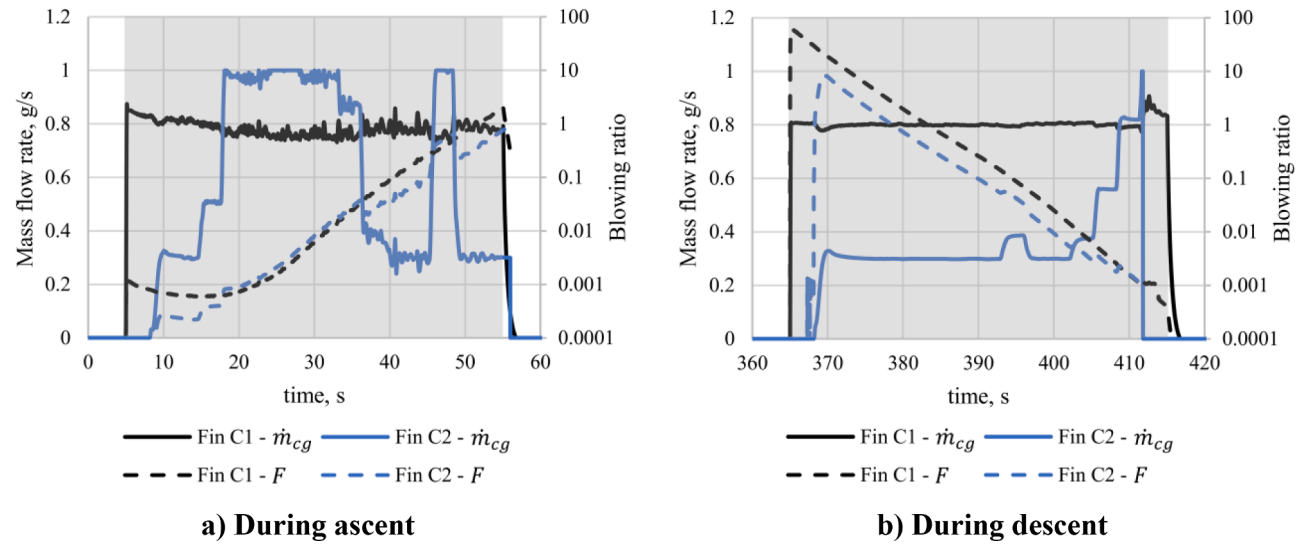

Fig. 12. Cooling gas mass flow rate and blowing ratio for the transpiration cooled fins.

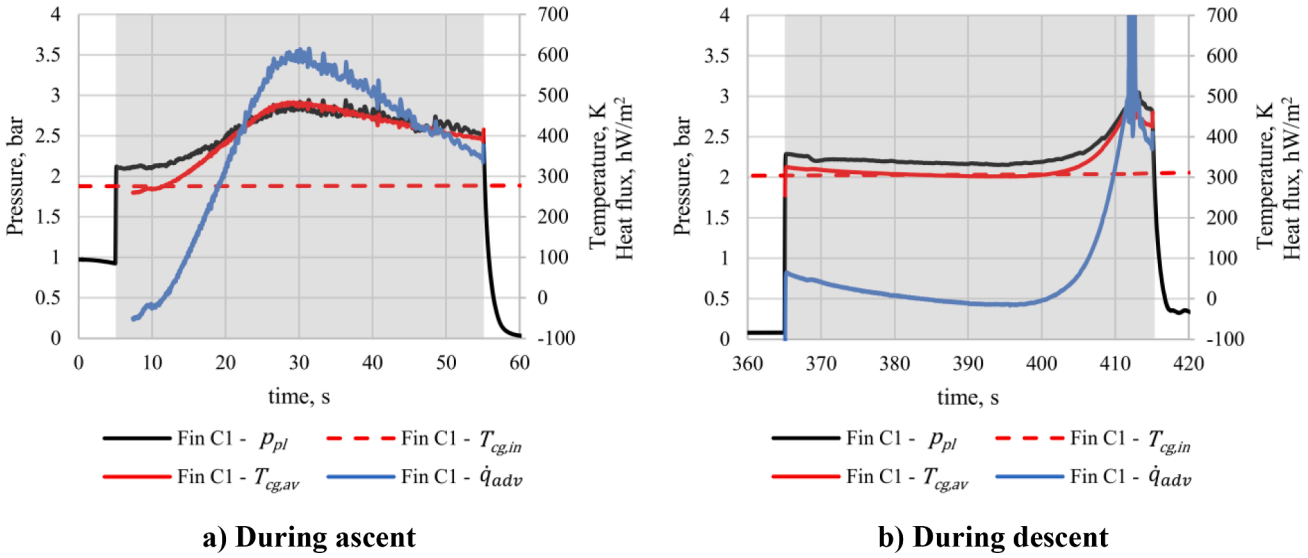

Fig. 13. Cooling gas conditions in the fin C1 and corresponding advection contribution.

done in [32], given by:

$$\Phi = \frac{T_{ref} - T_c}{T_{ref} - T_{cg,in}} \tag{6}$$

where T_c is the measured temperature in the transpiration-cooled fin, T_{ref} the corresponding measured reference temperature in the non-cooling conditions and $T_{cg,in}$ is the initial temperature of the cooling gas, as measured inside the fin's plenum.

6. Flight data and discussion

In this section, the main results of the FinEx module measured during the flight are shown and discussed.

As mentioned before, the operation of the transpiration cooling system was monitored by measuring the pressure and temperature along the gas feeding line downstream of the solenoid valve. As shown in Fig. 11, the pressure in the feeding line rises to the value of around 12.5 bar during the prescribed experimental window, between $T + 5$ s and $T + 55$ s and then again at $T + 365$ s, when the system activation signal is sent to open the solenoid valve. It can be observed that the pressure oscillates during the first activation interval, probably due to the vibrational load associated with the solid rocket motor operation, while the behavior is more stable during the second activation interval until motor separation. On the other side, the gas temperature shows a slight increase due to the slow heat conduction from the external surfaces to the inner parts of the payload.

The cooling gas mass flow rates in the two fins for the two experimental windows are shown in Fig. 12 together with the corresponding blowing ratio. For fin C1 the coolant mass flow rate is nearly constant in both experimental windows around a value of 0.8 g/s. For fin C2, the mass flow rate, regulated by the CATS, nominally starts from a value of 0.3 g/s and then it is increased according to the determined thermal load. Moreover, it is worth noticing that the trend of the blowing ratio is affected by the non-stationary character of the flow conditions. In fact, during the ascent, after a first period in which the acceleration roughly compensates for the effect of the density decrease with the increasing altitude, the velocity reaches a peak and then decreases too; therefore, the mass flux $\rho_e u_e$ decreases and the blowing ratio increases. The opposite happens during the descent.

As an example, Fig. 13 shows for the fin C1 the evolution of the

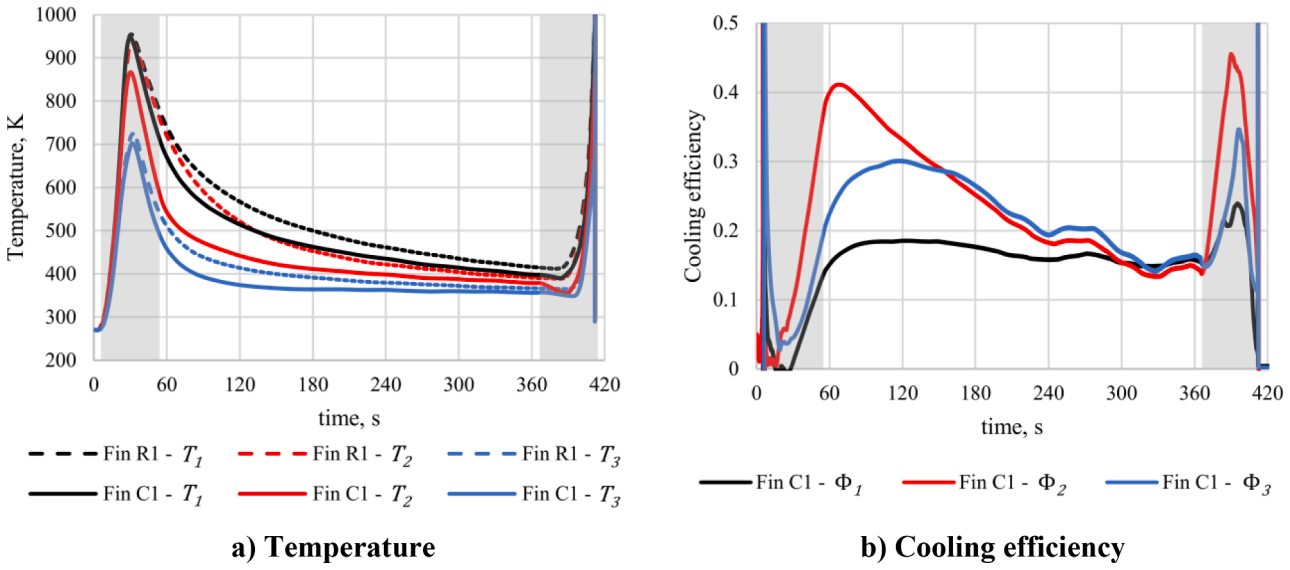

Fig. 14. Measured temperature on the Fin R1 and C1 and corresponding cooling efficiency.

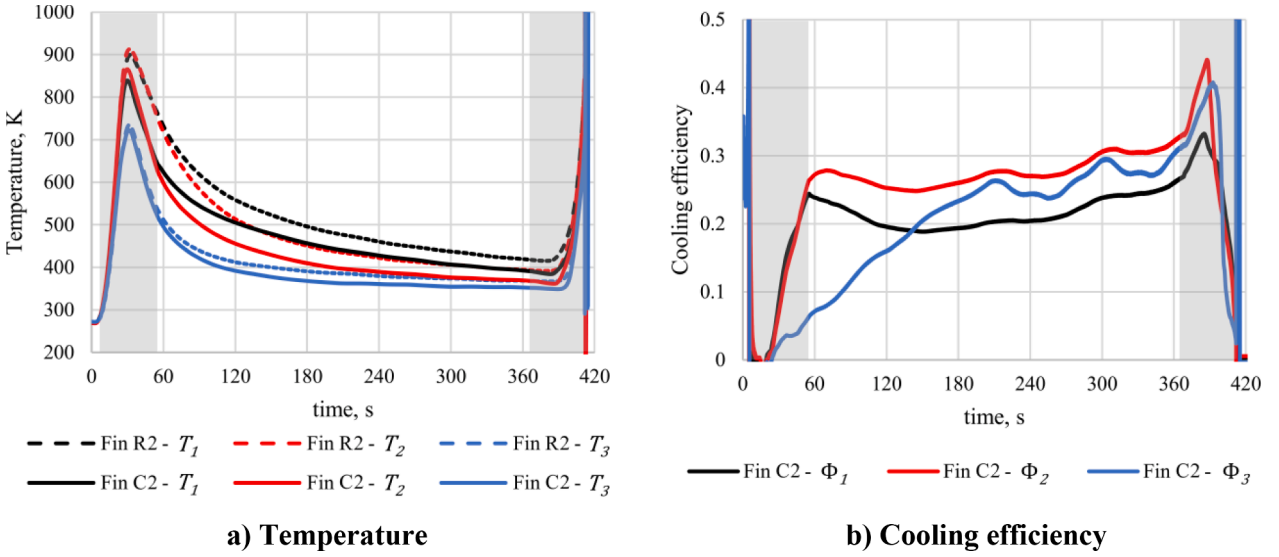

Fig. 15. Measured temperature on the Fin R2 and C2 and corresponding cooling efficiency.

pressure measured inside the plenum during the two experimental windows. In this case, in which the cooling gas mass flow rate is approximately constant, the behavior of the plenum pressure is directly connected to the evolution of the temperature of the gas within the fin, which in turn is affected by the fin thermal response [33]. In particular, when the fin heats up and the gas temperature correspondingly increases, the pressure in the plenum increases as well.

Furthermore, Fig. 13 shows also an estimation of the heat flux removed by advection, calculated with Eq. (4), in the simplified assumptions described in Section 5.

Fig. 14 shows the thermal response of the fins R1 and C1 in terms of the measured temperatures in the locations shown in Fig. 6 and the corresponding cooling efficiency obtained with the Eq. (6).

All the temperatures show a fast increase during the ascent phase reaching the maximum value at around 30 s, to successively decrease when higher altitudes are reached and the Mach number decreases. The temperatures measured on the cooled fin C1 are generally lower. The cooling efficiency grows continuously during the time of activation of the transpiration cooling, both because of the initially low value of the blowing ratio and because of the thermal inertia of the material, reaching a maximum at the end of the first experimental window. After the transpiration cooling is deactivated the temperature in the fin C1 stays lower but the difference reduces because the higher temperatures on the fin R1 cause a higher radiative heat dissipation. Finally, during the second activation interval the cooling efficiency rapidly grows again reaching a new peak around 393 s when the blowing ratio decreases below 0.1.

From Fig. 14b, it can also be noticed that the cooling efficiency corresponding to the TC1 measurement for the fin C1 is comparatively low. A possible explanation for this behavior is given by the shock wave that, as mentioned before, is forming on the camera cases present on the PSM in front of the fins R1 and C1. For higher Mach numbers a shock is estimated to be impinging on the upper region of the fins creating a localized higher pressure which in turn partially blocks locally the coolant effusion. The behavior in the location of TC3 is on the other side influenced by the proximity to the aluminum module body and the corresponding thermal conduction.

Finally, Fig. 15 shows the results for the fins R2 and C2. In general,

the qualitative behavior is similar to what is described above for the fins R1-C1. The main difference is given by the fact that, since the total mass flow rate of the coolant was lower, the resulting cooling efficiency is also lower. On the other side, it can be noticed that in this case, the thermal response during the activation of the transpiration cooling in the position of TC1 is similar to the response in the position of TC2. The reason is that, in this case, there is no shock wave impingement and the coolant outflow is presumably more uniform.

7. Conclusions

In the present work, the setup of the FinEx rocket module for the flight experiment of transpiration cooling applied to sharp leading-edge fins in a hypersonic regime and the corresponding main in-flight measured data are presented.

The module hosted four identical CMC fins whose leading edge was made of the innovative in-house developed OCTRA material, which is a variant of the C/C-SiC material with a predefined level of porosity to allow transpiration cooling. While two fins were uncooled as reference, the other two fins were connected to a gas system feeding gaseous nitrogen under predefined operating conditions. In particular, a constant mass flow rate was set for the fin C1, while a variable mass flow rate was foreseen for the fin C2 adjusted in real time by a specifically design control system adjusted according to the instantaneous actual thermal load.

The module was integrated into the HIFLIER sounding rocket, which was successfully launched from Esrange Space Center in Kiruna (Sweden) on the 10th October 2023. The rocket performed a parabolic trajectory reaching hypersonic velocities with a peak Mach number above 6.1 during the two experimental time intervals in the ascent and in the descent, during which the transpiration cooling system was activated.

The data measured during the flight show that the transpiration cooling worked correctly, activating the flow rate during the prescribed experimental windows. Moreover, the in-depth material temperatures measured for each fin on three different locations near the leading edge demonstrate the clear beneficial effect of the transpiration cooling, with cooling efficiency up to 30–40 %. Nevertheless, further analysis of the results also shows the need in case of future applications to take into account the strongly non-stationary character of the aerothermal conditions during the flight, differently to typical stationary laboratory experiments, and to introduce proper countermeasures in the case of complex aerodynamic phenomena, like shock wave impingement, can be foreseen, which can create non-uniform conditions and partial local effusion blocking.

Overall, the measured results represent a precious database for a better understanding of the behavior of transpiration cooling systems in real hypersonic flight conditions and further activities are already going on. This includes the reconstruction of the actual spatially-resolved heat fluxes from the measured temperatures with the Non-Integer System Identification method, the detailed analysis of the CATS system operation for the adjustment of the cooling gas mass flow rate according to the actual thermal load is analyzed in detail and the definition of a reliable numerical model for simulating the in-flight thermal behavior of the fins both taking into account the effect of the transpiration cooling.

CRediT authorship contribution statement

Giuseppe D. Di Martino: Writing – review & editing, Writing – original draft, Visualization, Validation, Supervision, Resources, Project administration, Methodology, Investigation, Formal analysis, Data curation, Conceptualization. **Jonas Peichl:** Writing – review & editing, Methodology, Investigation, Formal analysis. **Fabian Hufgard:** Writing – review & editing, Methodology, Data curation, Conceptualization. **Christian Duernhofer:** Writing – review & editing, Methodology, Data curation. **Stefan Loehle:** Writing – review & editing, Supervision, Methodology, Conceptualization. **Johannes Göser:** Writing – review & editing, Resources, Project administration, Investigation.

Declaration of competing interest

The authors declare that they have no known competing financial interests or personal relationships that could have appeared to influence the work reported in this paper.

Acknowledgments

The present work was carried out in the framework of the HIFLIER1 flight experiment project, primarily funded and coordinated by the US Air Force Research Laboratory (AFRL) and operated and launched by DLR Mobile Rocket Base (MORABA) in collaboration with the Swedish Space Corporation (SSC).

Furthermore, the authors wish to thank Matthias Scheiffele and Felix Vogel from the Ceramic Composite Structures department of DLR-BT, for the manufacturing of the raw materials, and Frank Entenmann from the Space System Integration department of DLR-BT for the machining of the fin and for the continuous technical support.

Data availability

Data will be made available on request.

References

[1] J.D. Anderson, Hypersonic and High-Temperature Gas Dynamics, 3rd ed., American Institute of Aeronautics and Astronautics, 2006 https://doi.org/10.2514/4.105142.
[2] H. Hald, H. Weihs, Safety Aspects of CMC Materials and Hot Structures, in: Proceedings of Joint ESA-NASA Space-Flight Safety Conference, ESA SP-486, 2002.
[3] A. Gülhan, D. Neeb, T. Thiele, F. Siebe, Aerothermal postflight analysis of the sharp edge flight experiment-II, J. Spacecraft Rockets 53 (2016) 153–177, https://doi.org/10.2514/1.A33275.
[4] W.M. Kays, Heat transfer to the transpired turbulent boundary layer, Int. J. Heat Mass Transf. 15 (5) (1972) 1023–1044, https://doi.org/10.1016/0017-9310(72)90237-2.
[5] W.H. Dorrance, F.J. Dore, The effect of mass transfer on the compressible turbulent boundary-layer skin friction and heat transfer, J. Aeronautical Sci. 21 (6) (1954) 404–410, https://doi.org/10.2514/8.3050.
[6] M.W. Rubesin, C.C. Pappas, An analysis of the boundary layer characteristics on a flat plate with disturbed light-gas injection, NACA TN 4149 (1958).
[7] A.V. Luikov, Heat and mass transfer in transpired cooling, Int. J. Heat Mass Transf. 6 (1963) 559–570, https://doi.org/10.1016/0017-9310(63)90013-9.
[8] D.E. Glass, A.D. Dilley, H.N. Kelly, Numerical analysis of convection/transpiration cooling, J. Spacecrafts Rockets 38 (1) (2001) 15–20, https://doi.org/10.2514/2.3666.
[9] T. Reimer, M. Kuhn, A. Gülhan, B. Esser, M. Sippel, A. van Foreest, Transpiration cooling tests of porous CMC in hypersonic flow, in: 17th AIAA International Space Planes and Hypersonic Systems and Technologies Conference, AIAA 2011-2251, 2011, https://doi.org/10.2514/6.2011-2251.
[10] S. Gulli, L. Maddalena, S. Hosder, Variable transpiration cooling for the thermal management of reusable hypersonic vehicles, Aerosp. Sci. Technol. 29 (1) (2013) 434–444, https://doi.org/10.1016/j.ast.2013.05.002.
[11] C. Dittert, C. Kütemeyer, et al., Octra - optimized ceramic for hypersonic application with transpiration cooling, in: M. Singh, T. Ohji, et al. (Eds.), Advances in High Temperature Ceramic Matrix Composites and Materials for Sustainable Development; Ceram. Transactions, Vol. 263, The American Ceramic Society, 2017, pp. 389–399, https://doi.org/10.1002/9781119407270.ch37.
[12] C. Dittert, H. Böhrk, S. Löhle, A transpiration cooled wedge with adapted permeability, in: HiSST: International Conference on High-Speed Vehicle Science Technology, 2018. Moscow, Russia.
[13] J. Peichl, A. Schwab, M. Selzer, H. Böhrk, J. von Wolfersdorf, Experimental investigation of transpiration cooling in a subscale combustion chamber with non-reactive flow, in: 2nd International Conference on High-Speed Vehicle Science & Technology, 2022. Bruges, Belgium.
[14] A. Gülhan, S. Braun, An experimental study on the efficiency of transpiration cooling in laminar and turbulent hypersonic flows, Exp. Fluids 50 (2011) 509–525, https://doi.org/10.1007/s00348-010-0945-6.
[15] J. Grzelak, P. Doerffer, T. Lewandowski, The efficiency of transpiration flow through perforated plate, Aerosp. Sci. Technol. 110 (2021) 106494, https://doi.org/10.1016/j.ast.2021.106494.
[16] I. Naved, T. Hermann, C. Hambidge, H.S. Ifti, C. Falsetti, M. McGilvray, I. S. Tirichenko, L. Vandeperre, Transpiration-cooling heat transfer experiments in laminar and turbulent hypersonic flows, J. Thermophys. Heat Transf. 37 (2) (2023) 281–295, https://doi.org/10.2514/1.T6626.

[17] S. Loehle, F. Zander, M. Eberhart, T. Hermann, A. Meindl, B. Massuti-Ballester, D. Leiser, F. Hufgard, A.S. Pagan, G. Herdrich, S. Fasoulas, Assessment of high enthalpy flow conditions for re-entry aerothermodynamics in the plasma wind tunnel facilities at IRS, CEAS Space J 14 (2022) 395–406, https://doi.org/10.1007/s12567-021-00396-y.
[18] R. Savino, L. Criscuolo, G.D. Di Martino, S. Mungiguerra, Aero-thermo-chemical characterization of ultra-high-temperature ceramics for aerospace applications, J. Eur. Ceram. Soc. 38 (8) (2018) 2937–2953, https://doi.org/10.1016/j.jeurceramsoc.2017.12.043.
[19] H. Böhrk, C. Dittert, H. Weihs, T. Thiele, A. Gülhan, Sharp leading edge at hypersonic flight: modeling and flight measurement, J. Spacecraft Rockets 51 (5) (2014) 1753–1760, https://doi.org/10.2514/1.A32892.
[20] S. Löhle, H. Böhrk, U. Fuchs, B. Kraetzig, H. Weihs, Three-dimensional thermal analysis of the HIFiRE-5 ceramic fin, in: 18th AIAA/3AF International Space Planes and Hypersonic Systems and Technologies Conference, AIAA 2012-5920, 2012, https://doi.org/10.2514/6.2012-5920.
[21] A. Gülhan, D. Hargarten, M. Zurkaulen, F. Klingenberg, F. Siebe, S. Willems, G. Di Martino, T. Reimer, Selected results of the hypersonic flight experiment STORT, Acta Astronaut 211 (2023) 333–343, https://doi.org/10.1016/j.actaastro.2023.06.034.
[22] H. Böhrk, Transpiration-cooled hypersonic flight experiment: setup, flight measurement, and reconstruction, J. Spacecraft Rockets 52 (3) (2015) 674–683, https://doi.org/10.2514/1.A33144.
[23] J. Ettl, D. Kim, A.P. Schmidt, J. Turner, Using data fusion of DMARS-R-IMU and GPS data for improving attitude determination accuracy, in: SpaceOps 2016 Conference, AIAA 2016-2637, 2016, https://doi.org/10.2514/6.2016-2637.
[24] U.S. Standard Atmosphere, 1976, U.S. Government Printing Office, Washington, D. C., 1976.
[25] G. Di Martino, J. Peichl, F. Hufgard, C. Duernhofer, S. Loehle, Setup of flight experiment of transpiration cooled sharp edge fins on the sounding rocket HIFLIER1, in: Aerospace Europe Conference 2023 –10TH EUCASS –9TH CEAS, 2023, https://doi.org/10.13009/EUCASS2023-005.
[26] G.D. Di Martino, H. Böhrk, J. Schäfer, C. Müller, J. Peichl, F. Hufgard, C. Duernhofer, S. Loehle, Design of the transpiration cooled fin experiment FinEx II on HIFLIER1, in: 2nd International Conference on High-Speed Vehicle Science Technology, 2022.
[27] R. Kochendorfer, N. Lutzenburger, H. Weihs, Joining techniques for fibre ceramic structures, Adv. Composites Letters 13 (1) (2004), https://doi.org/10.1177/096369350401300106.
[28] M.D.M. Innocentini, L.A. Nascimento, V.C. Pandolfelli, The pressure-decay technique for air permeability evalulation of dense refactory ceramics, Cement and Concrete Res. 34 (2004) 293–298, https://doi.org/10.1016/j.cemconres.2003.08.006.
[29] F. Hufgard, C. Duernhofer, S. Fasoulas, S. Loehle, Novel heat flux controlled surface cooling for hypersonic flight, Sci. Reports 13 (2023) 13109, https://doi.org/10.1038/s41598-023-40281-8.
[30] R.A. Hord, An approximate solution for axially symmetric flow over a cone with an attached shock wave, NACA Tech. Note 3485 (1955).
[31] F. Hufgard, C. Duernhofer, S. Fasoulas, S. Loehle, A transpiration cooled heat flux sensor utilizing plenum pressure: measurement in high enthalpy flow, in: 2nd International Conference on Flight Vehicles, Aerothermodynamics and *Re*-entry Missions & Engineering (FAR), 2022.
[32] T. Langener, J. von Wolfersdorf, J. Steelant, Experimental investigations on transpiration cooling for scramjet applications using different coolants, AIAA J 49 (7) (2011) 1409–1419, https://doi.org/10.2514/1.J050698.
[33] S. Loehle, S. Schweikert, J. von Wolfersdorf, Method for heat flux determination of a transpiration-cooled wall from pressure data, J. Thermophys. Heat Transf. 30 (3) (2016) 567–572, https://doi.org/10.2514/1.T4815.